

Gate-defined Kondo lattices with valley-helical quantum dot arrays

Antonio L. R. Manesco¹, [†]

1 Kavli Institute of Nanoscience, Delft University of Technology, Delft 2600 GA, The Netherlands
[†]am@antoniomanesco.org

Date here

Abstract

Kondo physics and heavy-fermion behavior has been predicted and observed in moiré materials. The electric tunability of moiré materials allows an *in-situ* study of Kondo lattices' phase diagrams, which is not possible with their intermetallic counterparts. However, moiré platforms rely on twisting, which introduces twisting angle disorder and undesired buckling. Here we propose device layouts for one- and two-dimensional gate-defined superlattices in Bernal bilayer graphene where localized states couple to dispersive valley-helical modes. We show that, under electronic interactions, these superlattices are described by an electrically-tunable Kondo-Heisenberg model.

1 Introduction

Kondo lattices are constituted by an array of magnetic moments coupled to a dispersive electron gas [1–3]. Historically, these lattices were first realized in intermetallic compounds, where localized *d* or *f* orbitals couple to dispersive bands leading to heavy fermion behavior [4]. The large charge density of these compounds screens electric fields, forbidding electrostatic tunability of the electron density. Therefore an exploration of the phase diagram requires the growth of several samples [5–12].

In the recent years, moiré materials became standard platforms to study correlated matter [13–15]. The quench of the kinetic energy caused by the moiré potential enhances the effects of electronic interactions, triggering correlated phases [16, 17]. In the past few years, moiré Kondo lattices have been both theoretically proposed and probed experimentally [18–22]. In contrast to their intermetallic counterparts, the electric tunability of moiré Kondo lattices allow *in situ* control of the phase diagram.

Despite their versatility and tunability, experiments in moiré materials lack quantitative reproducibility [23]. The mechanical manipulation required to fabricate moiré devices limit their quality. Thus, their electronic structures vary from one sample to the other. These fabrication issues also limit the scalability of moiré devices. Gate-defined superlattices overcome these limitations. The recent progress on patterning graphite gates allows manipulation of the superlattice potential without mechanical manipulation of the active material layer [24]. Moreover, unlike moiré materials, gate-defined superlattices are not constrained by the crystal lattice of the material.

Here we propose how gate-defined Bernal bilayer graphene superlattices as a platform for electrically controllable Kondo systems. Our proposal is inspired by recent experiments showing valley filtering via valley-helical channels [25–31]. We propose a gate geometry that creates a series of quantum dots coupled by these helical channels. We build a low-energy model for this device and show that, under electronic interactions, this Hamiltonian

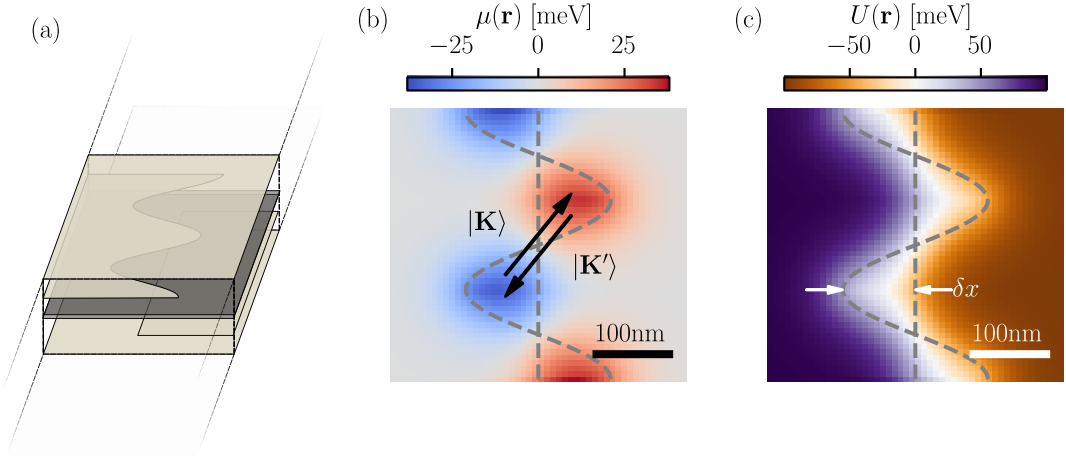


Figure 1: (a) Proposed device layout: a Bernal bilayer graphene sheet (black layers) with two top and two bottom gates. The outermost gates cover the full device, while the middle gate layers are patterned and screen the outer gates. The resulting chemical potential (a) and layer imbalance (b) result in a series of charge puddles with alternating polarities surrounded by a displacement field that flips direction from one side to the other of the device. The electrostatic profile creates a series of quantum dots coupled by valley-helical point contacts.

maps to a Kondo lattice. Finally, we extend this device to two-dimensional geometries. Our proposal is similar to Kondo lattices in twisted trilayer graphene [19], but in a fully electrically-defined setup.

2 Valley-helical quantum dot arrays

We present a scheme of the device in Fig. 1(a). Our layout consists of Bernal bilayer graphene with two bottom and two top gates, creating the chemical potential and displacement field landscapes shown in Fig. 1 (b, c). The regions with nonzero displacement field in Fig. 1 (b) result in a series of puddles with alternating polarity. These puddles are surrounded by regions with nonzero displacement field shown in Fig. 1(c). Because displacement fields gap the electronic structure of bilayer graphene (we review effects of displacement fields in Appendix B), the electrostatic profile results in a series of quantum dots with alternating polarity [32–39]. The connections between these quantum dots are point contacts constrained by regions with opposite displacement field. Since the valley Chern number flips sign with the displacement field (see Appendix B), these point contacts are valley-helical [25, 40, 41], as illustrated by the arrows in Fig. 1(b).

In Fig. 2 we show the low-energy bandstructure of a repeating unit cell of this device. We performed the tight-binding atomistic simulations using Kwant [42] and MeanFi [43] and provide all the details in the Appendix A. In Fig. 2(a) the bands are colored according to their inverse participation ratio (IPR). We observe that the presence of nearly flat bands with high IPR, which correspond to states localized in the charge puddles shown in Fig. 1(b). These localized states are weakly coupled to highly dispersive states. In Fig. 2(b) we show the valley-resolved bandstructure, where we can see that these dispersive states are valley helical. These states are weakly coupled to the dot levels with a strength $\Delta \sim \hbar v_F/\chi \sim 0.1 - 1 \text{ meV}$, where χ is the screening length of the electrostatic profile. These estimation of Δ agrees

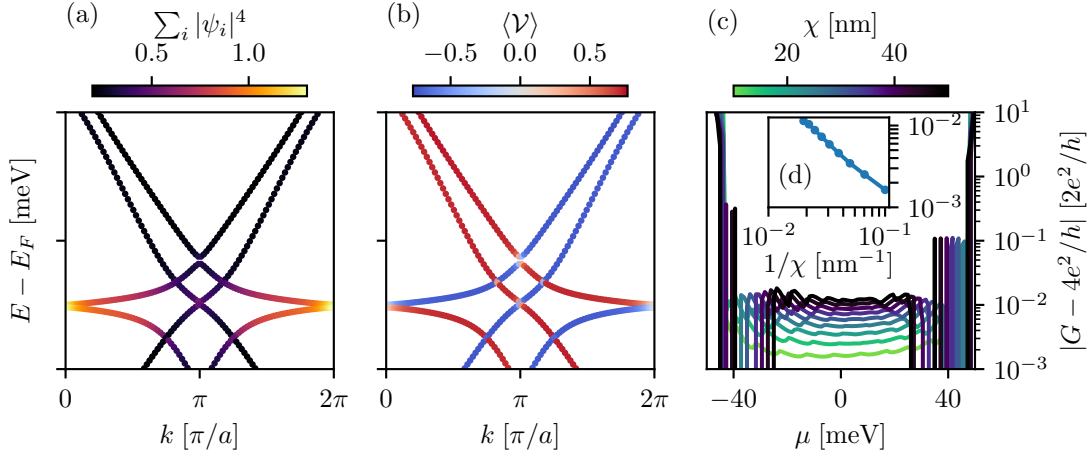


Figure 2: Bandstructure of a unit cell of the device shown in Fig. 1. In panel (a) the bandstructure is colored according to its inverse participation ratio (IPR), while in (b) the colors indicate valley polarization. We observe that localized states (with large IPR) couple to highly-dispersive valley-helical channels preserving valley number. (c) Conductance accross an unit cell of the device. We observe that $G \approx 4e^2/h$ indicating that the transport is dominated by the valley-helical channels. The inset shows the scaling of $|G - 4e^2/h|$ at $\mu = 0$ as a function of $1/\xi$. The scaling shown in the inset occurs due to the suppression of the overlap between dot levels.

with the observed anticrossings in the bandstructure. Because intervalley coupling depends on the small parameter $1/K\chi$, where K is the valley momentum, we observe that valley anticrossings are negligible

The dot levels at different charge puddles only couple through the valley helical states. We demonstrate the lack of direct interdot coupling computing the conductance accross an unit cells of this device. Since a perfectly helical point contact has a conductance $G = 4e^2/h$, we compute the difference $|G - 4e^2/h|$, shown in Fig. 2(c). The saturation of conductance at $4e^2/h$ indicates that only two helical valley states per spin channel propagate through the device. Moreover, in the inset of Fig. 2(c) we show the suppression of the conductance as a function of the screening length. Tunneling between the dots is suppressed by the displacement field. Thus, soft walls caused by large χ increase the overlap between the dot states, increasing tunneling of non-helical channels. Due to possible challenges on fabricating the multi-gated layout shown in Fig. 1(a), we suggest that an alternative layout with a single layer of split gates similar to a recent experimental realization is possible [31].

From the analysis above, we can construct a low-energy theory of helical states coupled to dot levels. We split the effective Hamiltonian in three terms

$$H(k) = H_{\text{helical}}(k) + H_{\text{dot}} + H_{\Delta}(k) . \quad (1)$$

Here, H_{helical} is the Hamiltonian of the helical states and reads

$$H_{\text{helical}}(k) = \sum_{\tau, \sigma, n} \tau(\delta\rho + v^\rho k) c_{\tau\sigma n}^\dagger(k) c_{\tau\sigma n}(k) \quad (2)$$

where v^ρ is the Fermi velocity of the helical mode ρ , δ is the splitting between the helical modes, τ is the valley index, σ is the spin index, and k is the momentum. The Hamiltonian

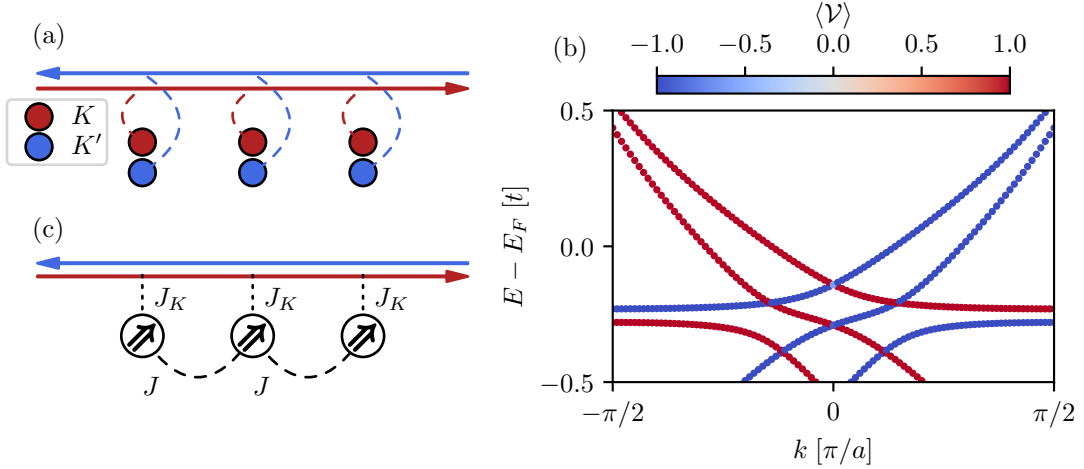


Figure 3: (a) Scheme of non-interacting model described by the Hamiltonian in Eq. 1. Helical valley states couple to dot levels preserving valley number. (b) Bandstructure from a lattice model of Eq. 1 using the tangent fermions approach. We recover the features of the bandstructure shown in Fig. 2 (b). (c) Scheme of low-energy interacting model. Due to a charging energy $V \gg \Gamma, \Delta$ we obtain a gate-tunable Kondo-Heisenberg model.

of the isolated dot levels is

$$H_{\text{dot}} = \epsilon \sum_{\tau\sigma} d_{\tau\sigma}^\dagger d_{\tau\sigma} \quad (3)$$

where ϵ_m is the energy of the dot levels. Finally, the valley-preserving coupling between helical and dot states is

$$H_\Delta(k) = \Delta \sum_{\tau,\sigma,\rho} d_{\tau\sigma}^\dagger c_{\tau\sigma\rho}(k) + h.c. \quad (4)$$

A scheme of this effective model is shown in Fig. 3 (a). We implement this model on a lattice using the tangent fermions approach [44, 45] (see Appendix C) and recover a dispersion similar to the one shown in Fig. 2 (b).

3 Effective Kondo lattice model

We now consider effects of electronic interactions. Interactions in the helical states only renormalize $v_F^{(n)}$ and are absorbed by $H_{\text{helical}}(k)$ [46–51]. Thus, we are left with the Coulomb interaction between dot levels

$$H_{\text{dot-dot}} = V \sum_{\tau,\tau'\sigma,\sigma'} n_{\tau\sigma} n_{\tau',\sigma'} , \quad (5)$$

where V is the charging energy of the quantum dots and $n_{\tau\sigma} = d_{\tau\sigma}^\dagger d_{\tau\sigma}$. We estimate that the charging energy is similar to other graphene quantum dots of comparable sizes, $U \sim 10\text{meV}$. Perturbative expansion over the small parameter Δ/U reduces the problem to an SU(4) Kondo model

$$H(k) \approx H_{\text{helical}}(k) + J_K \sum_i \mathbf{S}_i \cdot \mathbf{s}_i . \quad (6)$$

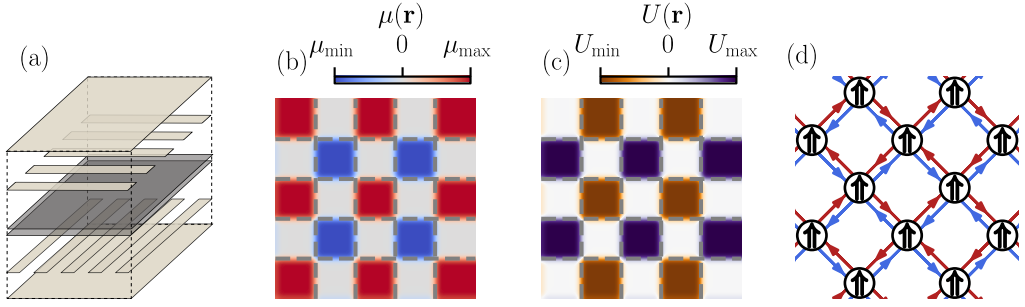


Figure 4: (a) Proposed device layout for a two-dimensional geometry. This layout results in the chemical potential landscape shown in (a) and layer imbalance shown in (b). The checkerboard pattern of charge puddles are connected by valley-helical point. (d) The low-energy description of this device consists of a series of localized moments in the quantum dots connnected by two copies of Chaker-Coddington networks with valley-dependent chirality.

with $J_K \sim \Delta^2/V$. Note that Kondo temperature of an $SU(N)$ lattice increases exponentially with N [52–58].

In the Hamiltonian of Eq. 1, we neglected the interdot tunneling rate Γ since it is exponentially suppressed by the gap caused by the displacement field. However, as discussed in Sec. 2, while Δ decreases, Γ increases with the screening length χ . Therefore the ratio Δ/Γ can be tunned with electrostatic engineering. Within the tunneling regime, $\Gamma/V \ll 1$, and we can again take the lowest order in perturbation theory, leading to an additional exchange coupling

$$H_{\text{exchange}} = J \sum_{\langle i,j \rangle} \mathbf{S}_i \cdot \mathbf{S}_j , \quad (7)$$

with $J \sim \Gamma^2/V$. Thus, this device is described by an electrically-tunable Kondo-Heisenberg Hamiltonian.

While we provide a gate layout for an one-dimensional system, this construction can be extended to two-dimensional lattices. In Fig. 4(a) we show a layout proposal for a two-dimensional lattice of quantum dots connected by valley-helical channels. This gate configuration creates a checkerboard landscape for the chemical potential and displacement field profiles, shown in Fig. 4 (b, c). The connections between the quantum dots results in two copies of a Chalker-Coddington network model [59] with valley-dependent chirality, *i.e.* a valley-helical network. Similar networks were predicted to existed in both twisted multilayers and strained graphene superlattices. Since we expect similar energy scales similar to the one-dimensional system in this two-dimensional lattice, a similar analysis results again in a gate-controllable Kondo-Heisenberg model.

4 Conclusion

We presented a strategy to obtain gate-defined graphene superlattices where quantum dots are coupled by valley helical quantum point contacts. We showed that the low-energy description of these superlattices maps to a electrically-tunable Kondo-Heisenberg Hamiltonian. We proposed a gate layouts for both one- and two-dimensional superlattices. Furthermore, we showed that the helical modes in two-dimensional superlattices form a

gate-defined valley-helical network model. Finally, we introduced a lattice description using the tangent fermions approach that can be used to simulate these superlattices with a reduced computational cost.

Acknowledgements

We acknowledge Kostas Vilkalis, Isidora Araya-Day, Anton Akhmerov, and Jose Lado for fruitful discussions. We also thank Valla Fatemi, Josep Ingla-Aynés, and Luca Banszerus for their input on the experimental implementation of our proposal. We thank Anton Akhmerov, Josep Ingla-Aynés, and Kushagra Aggarwal for the feedback on the manuscript.

Data availability

The code and data generated for this manuscript and additional datasets are fully available on Zenodo [60].

References

- [1] N. Mott, *Rare-earth compounds with mixed valencies*, Philosophical Magazine **30**(2), 403 (1974).
- [2] S. Doniach, *The kondo lattice and weak antiferromagnetism*, physica B+ C **91**, 231 (1977).
- [3] P. Coleman, *Heavy fermions and the kondo lattice: a 21st century perspective*, arXiv preprint arXiv:1509.05769 (2015).
- [4] K. Andres, J. E. Graebner and H. R. Ott, *4f-virtual-bound-state formation in ceal₃ at low temperatures*, Phys. Rev. Lett. **35**, 1779 (1975), doi:[10.1103/PhysRevLett.35.1779](https://doi.org/10.1103/PhysRevLett.35.1779).
- [5] F. Grosche, I. Walker, S. Julian, N. Mathur, D. Freye, M. Steiner and G. Lonzarich, *Superconductivity on the threshold of magnetism in cepd₂si₂ and cein₃*, Journal of Physics: Condensed Matter **13**(12), 2845 (2001).
- [6] J. Custers, P. Gegenwart, H. Wilhelm, K. Neumaier, Y. Tokiwa, O. Trovarelli, C. Geibel, F. Steglich, C. Pépin and P. Coleman, *The break-up of heavy electrons at a quantum critical point*, Nature **424**(6948), 524–527 (2003), doi:[10.1038/nature01774](https://doi.org/10.1038/nature01774).
- [7] S. Friedemann, T. Westerkamp, M. Brando, N. Oeschler, S. Wirth, P. Gegenwart, C. Krellner, C. Geibel and F. Steglich, *Detaching the antiferromagnetic quantum critical point from the fermi-surface reconstruction in ybrh₂si₂*, Nature Physics **5**(7), 465 (2009).
- [8] T. Park, F. Ronning, H. Yuan, M. Salamon, R. Movshovich, J. L. Sarrao and J. D. Thompson, *Hidden magnetism and quantum criticality in the heavy fermion superconductor cerhin5*, Nature **440**(7080), 65 (2006).
- [9] A. Schröder, G. Aeppli, R. Coldea, M. Adams, O. Stockert, H. Löhneysen, E. Bucher, R. Ramazashvili and P. Coleman, *Onset of antiferromagnetism in heavy-fermion metals*, Nature **407**(6802), 351–355 (2000), doi:[10.1038/35030039](https://doi.org/10.1038/35030039).

[10] H. Shishido, R. Settai, H. Harima and Y. Ōnuki, *A drastic change of the fermi surface at a critical pressure in cerhIn5: dhva study under pressure*, Journal of the Physical Society of Japan **74**(4), 1103 (2005).

[11] P. Gegenwart, T. Westerkamp, C. Krellner, Y. Tokiwa, S. Paschen, C. Geibel, F. Steglich, E. Abrahams and Q. Si, *Multiple energy scales at a quantum critical point*, Science **315**(5814), 969 (2007).

[12] S. Friedemann, N. Oeschler, S. Wirth, C. Krellner, C. Geibel, F. Steglich, S. Paschen, S. Kirchner and Q. Si, *Fermi-surface collapse and dynamical scaling near a quantum-critical point*, Proceedings of the National Academy of Sciences **107**(33), 14547–14551 (2010), doi:[10.1073/pnas.1009202107](https://doi.org/10.1073/pnas.1009202107).

[13] Y. Cao, V. Fatemi, A. Demir, S. Fang, S. L. Tomarken, J. Y. Luo, J. D. Sanchez-Yamagishi, K. Watanabe, T. Taniguchi, E. Kaxiras, R. C. Ashoori and P. Jarillo-Herrero, *Correlated insulator behaviour at half-filling in magic-angle graphene superlattices*, Nature **556**(7699), 80–84 (2018), doi:[10.1038/nature26154](https://doi.org/10.1038/nature26154).

[14] Y. Cao, V. Fatemi, S. Fang, K. Watanabe, T. Taniguchi, E. Kaxiras and P. Jarillo-Herrero, *Unconventional superconductivity in magic-angle graphene superlattices*, Nature **556**(7699), 43 (2018).

[15] E. Y. Andrei, D. K. Efetov, P. Jarillo-Herrero, A. H. MacDonald, K. F. Mak, T. Senthil, E. Tutuc, A. Yazdani and A. F. Young, *The marvels of moiré materials*, Nature Reviews Materials **6**(3), 201 (2021).

[16] R. Bistritzer and A. H. MacDonald, *Moiré bands in twisted double-layer graphene*, Proceedings of the National Academy of Sciences **108**(30), 12233 (2011).

[17] E. Y. Andrei and A. H. MacDonald, *Graphene bilayers with a twist*, Nature materials **19**(12), 1265 (2020).

[18] A. Kumar, N. C. Hu, A. H. MacDonald and A. C. Potter, *Gate-tunable heavy fermion quantum criticality in a moiré kondo lattice*, Physical Review B **106**(4), L041116 (2022).

[19] A. Ramires and J. L. Lado, *Emulating heavy fermions in twisted trilayer graphene*, Physical Review Letters **127**(2), 026401 (2021).

[20] A. Dalal and J. Ruhman, *Orbitally selective mott phase in electron-doped twisted transition metal-dichalcogenides: A possible realization of the kondo lattice model*, Physical Review Research **3**(4), 043173 (2021).

[21] D. Guerci, J. Wang, J. Zang, J. Cano, J. Pixley and A. Millis, *Chiral kondo lattice in doped mott2/wse2 bilayers*, Science Advances **9**(11), eade7701 (2023).

[22] V. Vaňo, M. Amini, S. C. Ganguli, G. Chen, J. L. Lado, S. Kezilebieke and P. Liljeroth, *Artificial heavy fermions in a van der waals heterostructure*, Nature **599**(7886), 582 (2021).

[23] C. N. Lau, M. W. Bockrath, K. F. Mak and F. Zhang, *Reproducibility in the fabrication and physics of moiré materials*, Nature **602**(7895), 41 (2022).

[24] L. A. Cohen, N. L. Samuelson, T. Wang, K. Klocke, C. C. Reeves, T. Taniguchi, K. Watanabe, S. Vijay, M. P. Zaletel and A. F. Young, *Nanoscale electrostatic control in ultraclean van der waals heterostructures by local anodic oxidation of graphite gates*, Nature Physics **19**(10), 1502–1508 (2023), doi:[10.1038/s41567-023-02114-3](https://doi.org/10.1038/s41567-023-02114-3).

[25] J. Li, K. Wang, K. J. McFaul, Z. Zern, Y. Ren, K. Watanabe, T. Taniguchi, Z. Qiao and J. Zhu, *Gate-controlled topological conducting channels in bilayer graphene*, *Nature Nanotechnology* **11**(12), 1060–1065 (2016), doi:[10.1038/nano.2016.158](https://doi.org/10.1038/nano.2016.158).

[26] Y. Kang, X. Ni, X. Cheng, A. B. Khanikaev and A. Z. Genack, *Pseudo-spin-valley coupled edge states in a photonic topological insulator*, *Nature Communications* **9**(1) (2018), doi:[10.1038/s41467-018-05408-w](https://doi.org/10.1038/s41467-018-05408-w).

[27] J. Li, R.-X. Zhang, Z. Yin, J. Zhang, K. Watanabe, T. Taniguchi, C. Liu and J. Zhu, *A valley valve and electron beam splitter*, *Science* **362**(6419), 1149–1152 (2018), doi:[10.1126/science.aa05989](https://doi.org/10.1126/science.aa05989).

[28] C. Park, *Magnetoelectrically controlled valley filter and valley valve in bilayer graphene*, *Phys. Rev. Appl.* **11**, 044033 (2019), doi:[10.1103/PhysRevApplied.11.044033](https://doi.org/10.1103/PhysRevApplied.11.044033).

[29] H. Chen, P. Zhou, J. Liu, J. Qiao, B. Oozyilmaz and J. Martin, *Gate controlled valley polarizer in bilayer graphene*, *Nature communications* **11**(1), 1202 (2020).

[30] K. Huang, H. Fu, K. Watanabe, T. Taniguchi and J. Zhu, *High-temperature quantum valley hall effect with quantized resistance and a topological switch*, *Science* **385**(6709), 657–661 (2024), doi:[10.1126/science.adj3742](https://doi.org/10.1126/science.adj3742).

[31] K. Davydov, X. Zhang, W. Ren, M. Coles, L. Kline, B. Zucker, K. Watanabe, T. Taniguchi and K. Wang, *Easy-to-configure zero-dimensional valley-chiral modes in a graphene point junction*, arXiv:2404.01027 (2024).

[32] E. McCann, *Asymmetry gap in the electronic band structure of bilayer graphene*, *Physical Review B* **74**(16) (2006), doi:[10.1103/physrevb.74.161403](https://doi.org/10.1103/physrevb.74.161403).

[33] E. V. Castro, K. S. Novoselov, S. V. Morozov, N. M. R. Peres, J. M. B. L. dos Santos, J. Nilsson, F. Guinea, A. K. Geim and A. H. C. Neto, *Biased bilayer graphene: Semiconductor with a gap tunable by the electric field effect*, *Phys. Rev. Lett.* **99**, 216802 (2007), doi:[10.1103/PhysRevLett.99.216802](https://doi.org/10.1103/PhysRevLett.99.216802).

[34] H. Min, B. Sahu, S. K. Banerjee and A. H. MacDonald, *Ab initiotheory of gate induced gaps in graphene bilayers*, *Physical Review B* **75**(15) (2007), doi:[10.1103/physrevb.75.155115](https://doi.org/10.1103/physrevb.75.155115).

[35] J. B. Oostinga, H. B. Heersche, X. Liu, A. F. Morpurgo and L. M. K. Vandersypen, *Gate-induced insulating state in bilayer graphene devices*, *Nature Materials* **7**(2), 151–157 (2007), doi:[10.1038/nmat2082](https://doi.org/10.1038/nmat2082).

[36] Y. Zhang, T.-T. Tang, C. Girit, Z. Hao, M. C. Martin, A. Zettl, M. F. Crommie, Y. R. Shen and F. Wang, *Direct observation of a widely tunable bandgap in bilayer graphene*, *Nature* **459**(7248), 820–823 (2009), doi:[10.1038/nature08105](https://doi.org/10.1038/nature08105).

[37] A. B. Kuzmenko, I. Crassee, D. van der Marel, P. Blake and K. S. Novoselov, *Determination of the gate-tunable band gap and tight-binding parameters in bilayer graphene using infrared spectroscopy*, *Phys. Rev. B* **80**, 165406 (2009), doi:[10.1103/PhysRevB.80.165406](https://doi.org/10.1103/PhysRevB.80.165406).

[38] K. F. Mak, C. H. Lui, J. Shan and T. F. Heinz, *Observation of an electric-field-induced band gap in bilayer graphene by infrared spectroscopy*, *Physical Review Letters* **102**(25) (2009), doi:[10.1103/physrevlett.102.256405](https://doi.org/10.1103/physrevlett.102.256405).

[39] R. T. Weitz, M. T. Allen, B. E. Feldman, J. Martin and A. Yacoby, *Broken-symmetry states in doubly gated suspended bilayer graphene*, *Science* **330**(6005), 812–816 (2010), doi:[10.1126/science.1194988](https://doi.org/10.1126/science.1194988).

[40] I. Martin, Y. M. Blanter and A. F. Morpurgo, *Topological confinement in bilayer graphene*, *Physical Review Letters* **100**(3) (2008), doi:[10.1103/physrevlett.100.036804](https://doi.org/10.1103/physrevlett.100.036804).

[41] J. Jung, F. Zhang, Z. Qiao and A. H. MacDonald, *Valley-hall kink and edge states in multilayer graphene*, *Physical Review B* **84**(7) (2011), doi:[10.1103/physrevb.84.075418](https://doi.org/10.1103/physrevb.84.075418).

[42] C. W. Groth, M. Wimmer, A. R. Akhmerov and X. Waintal, *Kwant: a software package for quantum transport*, *New Journal of Physics* **16**(6), 063065 (2014), doi:[10.1088/1367-2630/16/6/063065](https://doi.org/10.1088/1367-2630/16/6/063065).

[43] K. Vilkelis, R. J. Zijderveld, A. R. Akhmerov and A. L. Manesco, *MeanFi*, doi:[10.5281/zenodo.11149850](https://doi.org/10.5281/zenodo.11149850) (2024).

[44] R. Stacey, *Eliminating lattice fermion doubling*, *Phys. Rev. D* **26**, 468 (1982), doi:[10.1103/PhysRevD.26.468](https://doi.org/10.1103/PhysRevD.26.468).

[45] C. W. J. Beenakker, A. Donís Vela, G. Lemut, M. J. Pacholski and J. Tworzydło, *Tangent fermions: Dirac or majorana fermions on a lattice without fermion doubling*, *Annalen der Physik* **535**(7) (2023), doi:[10.1002/andp.202300081](https://doi.org/10.1002/andp.202300081).

[46] J. González, F. Guinea and M. Vozmediano, *Non-fermi liquid behavior of electrons in the half-filled honeycomb lattice (a renormalization group approach)*, *Nuclear Physics B* **424**(3), 595–618 (1994), doi:[10.1016/0550-3213\(94\)90410-3](https://doi.org/10.1016/0550-3213(94)90410-3).

[47] V. N. Kotov, B. Uchoa, V. M. Pereira, F. Guinea and A. H. Castro Neto, *Electron-electron interactions in graphene: Current status and perspectives*, *Reviews of Modern Physics* **84**(3), 1067–1125 (2012), doi:[10.1103/revmodphys.84.1067](https://doi.org/10.1103/revmodphys.84.1067).

[48] D. C. Elias, R. V. Gorbachev, A. S. Mayorov, S. V. Morozov, A. A. Zhukov, P. Blake, L. A. Ponomarenko, I. V. Grigorieva, K. S. Novoselov, F. Guinea and A. K. Geim, *Dirac cones reshaped by interaction effects in suspended graphene*, *Nature Physics* **7**(9), 701–704 (2011), doi:[10.1038/nphys2049](https://doi.org/10.1038/nphys2049).

[49] E. G. Mishchenko, *Effect of electron-electron interactions on the conductivity of clean graphene*, *Physical Review Letters* **98**(21) (2007), doi:[10.1103/physrevlett.98.216801](https://doi.org/10.1103/physrevlett.98.216801).

[50] D. E. Sheehy and J. Schmalian, *Quantum critical scaling in graphene*, *Physical Review Letters* **99**(22) (2007), doi:[10.1103/physrevlett.99.226803](https://doi.org/10.1103/physrevlett.99.226803).

[51] T. Stauber, P. Parida, M. Trushin, M. Ulybyshev, D. Boyda and J. Schliemann, *Interacting electrons in graphene: Fermi velocity renormalization and optical response*, *Physical Review Letters* **118**(26) (2017), doi:[10.1103/physrevlett.118.266801](https://doi.org/10.1103/physrevlett.118.266801).

[52] M.-S. Choi, R. López and R. Aguado, *Su(4) kondo effect in carbon nanotubes*, *Physical Review Letters* **95**(6) (2005), doi:[10.1103/physrevlett.95.067204](https://doi.org/10.1103/physrevlett.95.067204).

[53] M. Filippone, C. u. u. u. P. m. c. Moca, G. Zaránd and C. Mora, *Kondo temperature of su(4) symmetric quantum dots*, *Phys. Rev. B* **90**, 121406 (2014), doi:[10.1103/PhysRevB.90.121406](https://doi.org/10.1103/PhysRevB.90.121406).

[54] P. Coleman, *$\frac{1}{N}$ expansion for the kondo lattice*, *Phys. Rev. B* **28**, 5255 (1983), doi:[10.1103/PhysRevB.28.5255](https://doi.org/10.1103/PhysRevB.28.5255).

[55] A. Ramires and P. Coleman, *Supersymmetric approach to heavy fermion systems*, Physical Review B **93**(3) (2016), doi:[10.1103/physrevb.93.035120](https://doi.org/10.1103/physrevb.93.035120).

[56] A. Auerbach and K. Levin, *Kondo bosons and the kondo lattice: Microscopic basis for the heavy fermi liquid*, Phys. Rev. Lett. **57**, 877 (1986), doi:[10.1103/PhysRevLett.57.877](https://doi.org/10.1103/PhysRevLett.57.877).

[57] A. J. Millis and P. A. Lee, *Large-orbital-degeneracy expansion for the lattice anderson model*, Phys. Rev. B **35**, 3394 (1987), doi:[10.1103/PhysRevB.35.3394](https://doi.org/10.1103/PhysRevB.35.3394).

[58] D. P. Arovas and A. Auerbach, *Functional integral theories of low-dimensional quantum heisenberg models*, Phys. Rev. B **38**, 316 (1988), doi:[10.1103/PhysRevB.38.316](https://doi.org/10.1103/PhysRevB.38.316).

[59] J. Chalker and P. Coddington, *Percolation, quantum tunnelling and the integer hall effect*, Journal of Physics C: Solid State Physics **21**(14), 2665 (1988).

[60] A. L. Rigotti Manesco, *Gate-defined Kondo lattices with valley-helical quantum dot arrays*, doi:[10.5281/zenodo.13284474](https://doi.org/10.5281/zenodo.13284474) (2024).

[61] J. W. McClure, *Band structure of graphite and de haas-van alphen effect*, Phys. Rev. **108**, 612 (1957), doi:[10.1103/PhysRev.108.612](https://doi.org/10.1103/PhysRev.108.612).

[62] J. C. Slonczewski and P. R. Weiss, *Band structure of graphite*, Phys. Rev. **109**, 272 (1958), doi:[10.1103/PhysRev.109.272](https://doi.org/10.1103/PhysRev.109.272).

[63] J. W. McClure, *Theory of diamagnetism of graphite*, Phys. Rev. **119**, 606 (1960), doi:[10.1103/PhysRev.119.606](https://doi.org/10.1103/PhysRev.119.606).

[64] I. M. Flór, A. Lacerda-Santos, G. Fleury, P. Roulleau and X. Waintal, *Positioning of edge states in a quantum hall graphene pn junction*, Physical Review B **105**(24) (2022), doi:[10.1103/physrevb.105.l241409](https://doi.org/10.1103/physrevb.105.l241409).

[65] J. Li, H.-B. Leng, H. Fu, K. Watanabe, T. Taniguchi, X. Liu, C.-X. Liu and J. Zhu, *Superconducting proximity effect in a transparent van der waals superconductor-metal junction*, Physical Review B **101**(19) (2020), doi:[10.1103/physrevb.101.195405](https://doi.org/10.1103/physrevb.101.195405).

[66] M. I. Katsnelson, K. S. Novoselov and A. K. Geim, *Chiral tunnelling and the klein paradox in graphene*, Nature Physics **2**(9), 620–625 (2006), doi:[10.1038/nphys384](https://doi.org/10.1038/nphys384).

[67] M. I. Katsnelson, *Graphene: carbon in two dimensions*, Materials Today **10**(1), 20 (2007), doi:[https://doi.org/10.1016/S1369-7021\(06\)71788-6](https://doi.org/10.1016/S1369-7021(06)71788-6).

A Model and simulation details

All the numerical simulations presented in this manuscript were obtained via a tight-binding implementation of Bernal-stacked bilayer graphene. The tight-binding model was implemented in Kwant [42], following the Slonczewski-Weiss-McClure parametrization [61–63] and using tight-binding parameters obtained via infrared spectroscopy [37]. We neglect the effects of spin-orbit coupling and therefore treat spins as a trivial degeneracy. Besides the pristine Slonczewski-Weiss-McClure tight-binding Hamiltonian $\mathcal{H}_{\text{pristine}}$, we add onsite modulations of the chemical potential μ and sublattice imbalance U to emulate the effects of multiple gate layers as

$$\mathcal{H}_{\text{onsite}} = \sum_n \psi_n^\dagger [U(\mathbf{r}_n) \text{sign}(\mathbf{r}_n \cdot \hat{z}) - \mu(\mathbf{r}_n)] \psi_n, \quad (8)$$

where $\psi_n = (c_n, c_n)^T$, c_n is an annihilation operator of an electron at the atomic site n .

Throughout the manuscript, we simulate mesoscopic devices with sizes $\sim 1\mu\text{m}$. To minimize the cost of the simulations, we rescale the tight-binding model by increasing the lattice constant as $\tilde{a} \mapsto sa$ and then adjusting the hopping parameters to preserve the low-energy Hamiltonian. We set $s = 10$ in the transport simulations and $s = 20$ in the bandstructure simulations due to their larger computational cost.

The screening effects are included by smoothening the electrostatic potential. In our calculations, we set the potential at the interface between two regions with potentials V_1 and V_2 as

$$V(\mathbf{r}) = \frac{(V_1 - V_2)}{2} \left[1 + \tanh \left(\frac{|\mathbf{r} - \mathbf{r}_B|}{\chi} \right) \right] + V_2, \quad (9)$$

where χ is the screening length, and \mathbf{r}_B is the closest point at the boundary between the two regions. Typically $\chi \sim 25 - 50\text{nm}$ and we use $\chi = 25\text{nm}$ throughout the manuscript except if it is explicitly stated [64, 65]. Thus, the chemical potential is the average between the potential in the two layers

$$\mu(\mathbf{r}) = \frac{V_{\text{upper}}(\mathbf{r}) + V_{\text{lower}}(\mathbf{r})}{2}, \quad (10)$$

and the layer imbalance is the difference between the layer potentials

$$U(\mathbf{r}) = V_{\text{upper}}(\mathbf{r}) - V_{\text{lower}}(\mathbf{r}). \quad (11)$$

We fix $U(\mathbf{r}) = \pm 100\text{meV}$ far from the gate edges through the manuscript.

We compute the conductance across the devices via scattering formalism. All the calculations are performed at zero bias. For the two-terminal devices simulated in the manuscript, the zero-bias conductance is

$$G = \frac{2e^2}{h} \text{Tr}(tt^\dagger), \quad (12)$$

where t is the transmission matrix, and the factor of 2 comes from spin degeneracy.

B Gate-defined valley-helical channels

Due to a combination of mirror and time-reversal symmetries, the conduction and valence bands in graphene are degenerate at the corners of the Brillouin zone, as shown in Fig. 5 (a). This degeneracy makes graphene a gapless semiconductor. Thus, modulations of the carrier

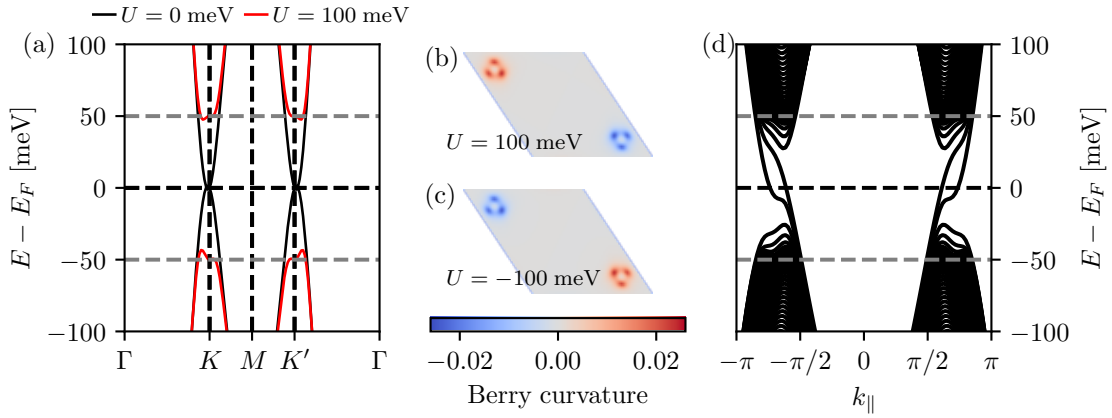


Figure 5: (a) Bulk bandstructure of Bernal bilayer graphene with $U_0 = 0$ and $U_0 = 100$ meV. A sublattice imbalance U_0 opens a gap in the band structure. Berry curvature for (b) $U_0 = 100$ meV and (c) $U_0 = -100$ meV. Due to time-reversal symmetry, the two valleys have opposite Berry curvature. However, the Berry curvature changes sign with layer imbalance. The valley Chern number changes across an interface where U flips sign results in the in-gap valley helical modes shown in panel (d).

density are insufficient to confine electrons due to Klein tunneling [66, 67]. However, in graphene multilayers, the mirror symmetry is broken by the application of an out-of-plane electric field. The potential imbalance U between the layers opens a gap in the electronic structure [32–38] as depicted by Fig. 5 (a). Therefore, it is possible to control the band gap of graphene multilayers with double-gated devices [38, 39].

In Bernal bilayer graphene, the Berry curvature at each valley depends on the direction of the external electric field, shown in Fig. 5 (b, c). Thus, at the interface of two regions with opposite displacement fields, the valley Chern number changes. As a consequence, these interfaces host topological valley helical channels. In Fig. 5 (d) we show the dispersion of a nanoribbon with a switching layer imbalance. Due to the valley Chern number switch at this interface, in-gap valley-helical states propagate along the interface [25, 40, 41]. The helicity of these channels thus constrains the electronic motion in a single direction. For this reason, these channels were proposed as valley filters.

C Lattice implementation

Here we present a lattice model that describes the low-energy behavior of the superlattices described throughout the text. We perform a lattice regularization of the Hamiltonian in Eq. 1 without fermion doubling following the tangent fermion approach [44, 45]. The core idea of this approach is obtaining a tangent dispersion for the helical states that can be expressed in a lattice as a generalized eigenproblem $H\Psi = E S \Psi$. Particularly, for the Hamiltonian in Eq. 1, we write for the helical

$$H_{\text{helical}} = i \sum_{i, \tau, \rho} \tau [\delta |i, \tau, \rho\rangle_h \langle i, \tau, \rho|_h + (t + \rho \delta t) |i + 1, \tau, \rho\rangle_h \langle i, \tau, \rho|_h] \quad (13)$$

with $t = (v^+ + v^-)/2a$, $\delta t = (v^+ - v^-)/2a$. The dot Hamiltonian follows trivially,

$$H_{\text{dot}} = \epsilon \sum_{i, \tau} |i, \tau\rangle_d \langle i, \tau|_d \quad (14)$$

and the coupling between helical states is

$$H_\Delta = \Delta \sum_{i,\tau,\rho} |i, \tau, \rho\rangle_h \langle i, \tau|_d + h.c. . \quad (15)$$

We used the subindices d and h to distinguish states in the dot chain and helical lattice. The overlap matrix of dot states corresponds to an orthogonal basis

$$S_{\text{dot}} = \sum_{i,\tau} |i, \tau\rangle_d \langle i, \tau|_d . \quad (16)$$

whereas for the helical modes

$$S_{\text{helical}} = \sum_{i,\tau,\rho} |i + 1, \tau, \rho\rangle_h \langle i, \tau, \rho|_h \quad (17)$$

Solving this generalized eigenproblem with periodic boundary conditions result in the spectrum shown in Fig. 2 (c). While the approach results in a single Dirac cone at $k = 0$, the tangent dispersion has a cusp at $k = \pm\pi$, and for this reason we plot the dispersion in Fig. 2 (c) within $[-\pi/2, \pi/2]$.